

Density engineering via inter-condensate dipole-dipole interactions: axial confinement and supersolids

Pranay Nayak,^{1,2} Ratheejit Ghosh,¹ and Rejish Nath¹

¹Department of Physics, Indian Institute of Science Education and Research, Pune 411 008, Maharashtra, India

²Department of Physics, Stockholm University, SE-10691 Stockholm, Sweden

(Dated: September 25, 2023)

Exploiting the long-range and anisotropic nature of dipole-dipole interactions, we show that the density of a *target* dipolar Bose-Einstein condensate can be engineered and axially confined using a trapped *control* dipolar condensate. Increasing the number of control condensates leads to exotic ground state structures, including supersolids and an incoherent array of density peaks. Single and double-peaked periodic structures are observed as a function of spacing between the control condensates. Our ideas may be generalized to engineer any other dipolar quantum system using another one of a similar dipole character. For instance, a Rydberg atom with electric dipole moment may be confined and manipulated using a trapped polar molecule and vice versa via long-range dipole-dipole interactions.

I. INTRODUCTION

The anisotropic and long-range nature of the dipole-dipole interactions (DDIs) led to a rich physics in dipolar quantum gases [1–4]. In particular, multi-dimensional bright solitons [5–9] and ground states with density patterns [10] remain a focus of study in dipolar Bose-Einstein condensates (DBECs). The discovery of dipolar quantum droplets [11–16], resulting from the interplay between contact and dipolar interactions, together with the quantum stabilization [17, 18] led to a lot of exciting developments in the recent past. The most remarkable among them is the observation of incoherent arrays of droplets and droplet supersolids [19–30]. The coherence in a droplet supersolid can be probed via excitations [23, 24, 26, 31] and the quantum moment of inertia [28]. More exotic and multi-dimensional supersolids are also predicted to exist in BECs [16, 30, 32–40].

An array of disconnected dipolar quantum gases exhibit collective phenomena because of the long-range DDIs [3, 41–44]. In condensates, they include dipolar drag [45, 46], hybrid excitations [47–49], soliton complexes [50–55], and coupled density patterns [56]. Also, the inter-layer interactions can significantly affect the stability of an atomic dipolar condensate, even for a small atomic dipole moment, as shown in a chromium BEC ($6\mu_B$ with μ_B the Bohr magneton for a chromium atom) [57, 58]. Remarkably, a recent experiment using cold gas of dysprosium atoms ($10\mu_B$) demonstrated strong inter-layer dipolar effects by reducing the layer separations to 50 nm from typical lattice spacings of 500 nm [59], opening up new directions in the physics of dipolar gases and possibly observe various exotic bilayer phenomena [45, 48, 60–71].

In this paper, we analyze the ground state of spatially disconnected dipolar condensates, in which one condensate is a *target* BEC, and the rest are *control* BECs. We assume the control BECs are confined in all directions. We aim to engineer the density of an axially unconfined target BEC via the inter-condensate DDIs. The parameter regimes are taken such that the corrections to the chemical potential from the quantum fluctuations or the Lee-Huang-Yang (LHY) corrections in each condensate are negligible [72, 73]. First, using a single

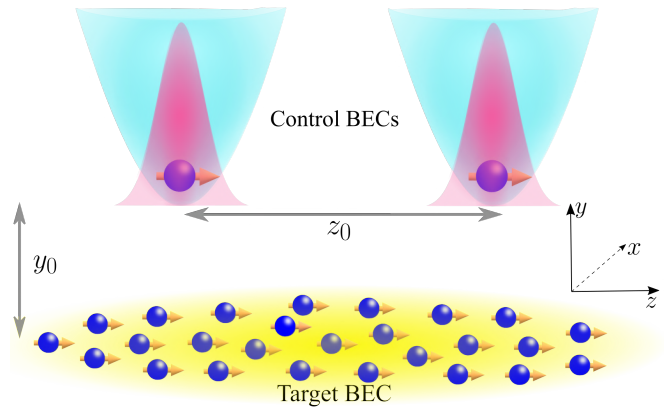


Figure 1. (color online). The schematic picture of the setup consists of three non-overlapping dipolar condensates. The two condensates in the top row, separated by a distance of z_0 , are the control BECs, whereas the bottom one is the target BEC. The target BEC is separated by a distance of y_0 from the control ones along the y -axis. The control BECs are confined in all directions, whereas the target one is axially (along z -axis) unconfined.

control BEC, we show that inter-tube DDIs can axially confine the target BEC, leading to a quasi-one-dimensional condensate with a density minimum at its center. The axial width and the peak density of the target BEC can be controlled by tuning the trap aspect ratio of the control BEC.

Increasing the number of control BECs imprints nontrivial density patterns in the target one. Strikingly, such density patterns can be further engineered. For instance, in a setup consisting of two control BECs, the target condensate undergoes a structural transition from a three-peaked ground state to a four-peaked one when the separation between the control BECs is varied. Interestingly, a periodic array of control BECs induces an effective periodic potential to the target BEC, forming various periodic density patterns. Three-dimensional numerical analysis of the coupled Gross-Pitaevskii equations reveals a periodic arrangement of single and double-peaked periodic structures forming coherent (supersolids) and incoherent density waves. Supersolids here are not created via quantum stabilization. But are similar to those discussed

in binary dipolar condensates in which one component supports the density modulation in the other component [74, 75]. Again, by adjusting the separation between the control BECs, the superfluid fraction of the supersolid can be modified but exhibits a nontrivial dependence. Ultimately, we propose an alternative approach to engineer dipolar condensates, primarily via inter-condensate DDIs, and may also find applications in other dipolar systems of the same dipole character, for instance, in a hybrid system of a polar molecule and a Rydberg atom, both having an electric dipole moment [76]. The properties of a polar molecule can be engineered or even confined using a Rydberg atom and vice versa.

The paper is structured as follows. The setup and model are introduced in Sec. II. In Sec. III, we discuss the axial confinement of the target dipolar BEC using a single control BEC. The density engineering using two control BECs is discussed in Sec. IV. The formation of periodic density peaks, including the supersolids in the target BEC due to an array of control BECs, is discussed in Sec. V. The experimental parameters for the state-of-the-art dipolar BECs are provided in Sec. VI. Finally, we summarize and provide an outlook in Sec. VII.

II. SETUP AND MODEL

The setup consists of M spatially disconnected dipolar condensates where one is a target BEC, and the rest are control BECs. The control BECs are confined in all three directions, whereas the target one is not axially confined, but the radial trapping potential is the same as that of the control ones. A schematic setup for $M = 3$ is shown in Fig. 1. The two condensates in the upper row are the control BECs, and the bottom one, separated by a distance of y_0 in the transverse y -direction, is the target BEC. Let N_t and N_c be the number of bosons in the target and control BECs, respectively. Each boson has a mass m and dipole moment d oriented along z axis [see Fig. 1]. At very low temperatures, the system is described in the mean field by coupled non-local Gross-Pitaevskii equations (NLGPEs),

$$i\hbar \frac{\partial}{\partial t} \psi_j(\mathbf{r}, t) = \left(-\frac{\hbar^2}{2m} \nabla^2 + V_j(\mathbf{r}) + g N_j |\psi_j(\mathbf{r}, t)|^2 + \sum_{i=1}^M N_i \int d^3 r' V_d(r - r') |\psi_i(r', t)|^2 \right) \psi_j(\mathbf{r}, t) \quad (1)$$

where ψ_j is the wavefunction of the j th condensate satisfying $\int |\psi_j(\mathbf{r})|^2 d^3 r = 1$, $N_j \in \{N_t, N_c\}$ and $V_j(\mathbf{r})$ is its external potential. The trapping potential experienced by a control BEC is $V_j(\mathbf{r}) = m\omega_\perp^2[x^2 + (y - y_0)^2]/2 + m\omega_z^2(z - z_j)^2/2$, where ω_\perp and ω_z are the trapping frequencies along the radial and axial directions and that of the target BEC is $V_j(\mathbf{r}) = m\omega_\perp^2(x^2 + y^2)/2$. The parameter $g = 4\pi\hbar^2 a_s/m$ quantifies the contact interaction strength with $a_s > 0$ being the s -wave scattering length. The dipolar potential is $V_d(r) = g_d(1 - 3\cos^2\theta)/r^3$, where $g_d \propto d^2$ and θ is the angle between the dipole and radial vectors. We introduce the dimensionless parameters $\tilde{g} = gN/\hbar\omega_\perp l_\perp^3$ and $\tilde{g}_d = g_d N / \hbar \omega_\perp l_\perp^3$ to quantify the interaction strengths, where $l_\perp = \sqrt{\hbar}/m\omega_\perp$. The contact interaction strength g is

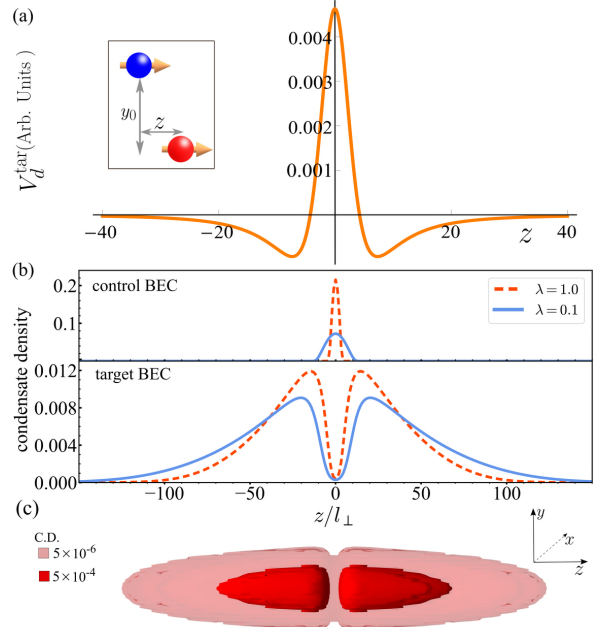


Figure 2. (color online). (a) The double-well dipolar potential $V_d^{\text{tar}}(z)$ acting on the target dipole (bottom, red) due to the control dipole (top, blue) as a function of the separation z . (b)-(c) Condensate densities for $M = 2$. (b) The integrated column density along the z -axis of the control and target BECs for $y_0 = 6l_\perp$, $\tilde{g} = 210$, and $\tilde{g}_d = 50$. Dashed lines are for $\lambda = 1$, and solid lines are for $\lambda = 0.1$. (b) The iso-surface density plot of the target BEC for $\lambda = 1$ reveals the axial confinement. C.D. stands for condensate density.

taken sufficiently large to ensure each condensate is dynamically stable, which also rules out the self-trapping of the target BEC along the axial direction [50]. The ground states of the complete system are obtained by solving the coupled three-dimensional NLGPEs in Eq. (1) via imaginary time evolution.

III. INTER-CONDENSATE AXIAL CONFINEMENT

First, we consider the minimal setup of $M = 2$, with one control and a target BEC. Before proceeding with condensates, we examine the dipolar potential between two point dipoles as shown in Fig. 2(a). The position of the top (control) dipole is fixed at $(y = y_0, z = 0)$, and the bottom (target) dipole can freely move along the z -axis. The potential experienced by the target dipole due to the control dipole is $V_d^{\text{tar}}(z) \propto (y_0^2 - 2z^2)/(y_0^2 + z^2)^{5/2}$. $V_d^{\text{tar}}(z)$ has a finite repulsive barrier centered at $z = 0$, followed by a local minimum on either side. At long distances, the potential decays to zero but is attractive, which leads to the axial confinement of the target dipole. Effectively, the spatially confined control dipole induces a double well potential on the target dipole.

The axial confinement of the target BEC is demonstrated in Fig. 2(b), where we show the density of control (top row) and target (bottom) condensates along the z axis for two different trap aspect ratios $\lambda = \omega_z/\omega_\perp$. The axial harmonic trap makes the peak density of the control BEC larger than that

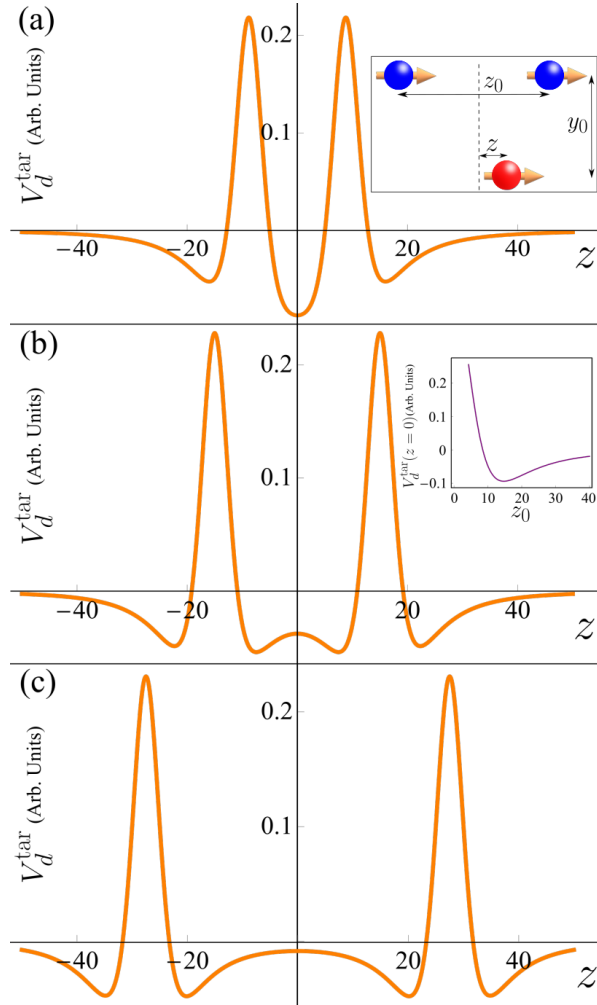


Figure 3. (color online). The dipolar potential $V_d^{\text{tar}}(z)$ (in arbitrary units) on the target dipole due to the two control dipoles. The inset of (a) shows the schematic of the three-point dipoles in which the two control dipoles (blue) on the top row are fixed at a separation of z_0 , and z determines the position of the target dipole (red) in the bottom. $V_d^{\text{tar}}(z)$ for (a) $z_0 = 15$, (b) $z_0 = 30$ and (c) $z_0 = 55$ are shown. The inset of (b) shows $V_d^{\text{tar}}(z = 0)$ as a function of z_0 , which exhibits a non-monotonous behavior.

of the target BEC and also axially shorter. The repulsive barrier in $V_d^{\text{tar}}(z)$ creates a density minimum at the center ($z = 0$) of the target BEC. The interplay between the attractive intra- and inter-condensate DDIs, the repulsive contact interactions, and kinetic energy leads to the axial confinement of the target BEC. As seen in Fig. 2(b), the axial width and peak density of the target BEC can be controlled by varying the aspect ratio λ . The more tightly we confine the control BEC, the larger the peak density and the lesser the axial width of the target BEC.

IV. DENSITY ENGINEERING OF THE TARGET BEC

Increasing the number of control BECs helps to engineer the density of the target BEC into more exotic patterns. To

demonstrate that, we use the setup shown in Fig. 1, for which $M = 3$. As shown below, the density patterns depend critically on z_0 , the separation between the two control BECs. To get an intuitive picture, we again look at the dipolar potential of three-point dipoles in a geometry identical to the BEC setup. The dipolar potential experienced by the target dipole (bottom) due to two control dipoles (top) placed at $\pm z_0/2$ is,

$$V_d^{\text{tar}}(z) \propto \frac{2y_0^2 - (z_0 - 2z)^2}{[4y_0^2 + (z_0 - 2z)^2]^{5/2}} + \frac{2y_0^2 - (z_0 + 2z)^2}{[4y_0^2 + (z_0 + 2z)^2]^{5/2}}. \quad (2)$$

In Fig. 3, we show $V_d^{\text{tar}}(z)$ as a function of z for three different z_0 . It has two maxima at $\pm z_0/2$ due to the repulsion from the control dipoles. There is a minimum on either side of the maxima, and the total number of minima depends on z_0 . The nature of potential at $z = 0$ also depends critically on z_0 . For smaller values of z_0 , $V_d^{\text{tar}}(z)$ exhibits a minimum at $z = 0$ [see Fig. 3(a)] and as z_0 increases, the minimum gets deeper. A further increase in z_0 , the minimum turns into a local maximum, resulting in two more minima on either side of $z = 0$ [see Fig. 3(b)]. For larger z_0 , the width of the central maximum increases, pushing the minima away from the center ($z = 0$), resulting in a pair of double-well potential [see Fig. 3(c)]. Each pair can be seen as emerging from each control dipole, similar to that of Fig. 2(a). The inset of Fig. 3(b) shows $V_d^{\text{tar}}(z = 0)$ as a function of z_0 , which exhibits a non-monotonous behavior as expected. In short, the dipolar potential acting on the target dipole can be engineered by varying the separation between the control dipoles. In particular, $V_d^{\text{tar}}(z)$ exhibits three local minima for small z_0 and four minima as z_0 becomes larger.

The effect of z_0 on the ground state density of the target BEC (n^{tar}) is shown in Fig. 4. The inter-condensate DDIs axially confine the target condensate. In Fig. 4(a), we plot the central density of the target BEC as a function of z_0 , which exhibits a non-monotonous behavior possessing a maximum, as expected from the nature of $V_d^{\text{tar}}(z = 0)$ shown in the inset of Fig. 3(b). For sufficiently small z_0 , we get a three-peak structure [see Fig. 4(b)]. Upon increasing z_0 , the central peak gets broader and denser [Fig. 4(c)] since the minimum of the potential at $z = 0$ gets deeper. Above a particular value, an increase in z_0 reduces the central density. Once $V_d^{\text{tar}}(z = 0)$ turns into a local maximum, the central density lobe develops a modulation [see Fig. 4(d)]. As z_0 increases further, the central peak breaks into two. [see Figs. 4(e) and 4(f)]. Hence, at large z_0 , a pair of semi-ellipsoid condensates is formed on either side of $z = 0$, leading to a four-peaked ground state density profile. The separation between the pairs can be made larger by incrementing z_0 .

We have taken the same number of atoms in both target and control BECs in the above scenarios. For a sufficiently small number of atoms in the target BEC, a single ellipsoid-shaped condensate is formed in the region between the target condensates, as shown in Fig. 5. In Fig. 5, we show the densities of both the control (two peaks on the top) and target (bottom) condensates.

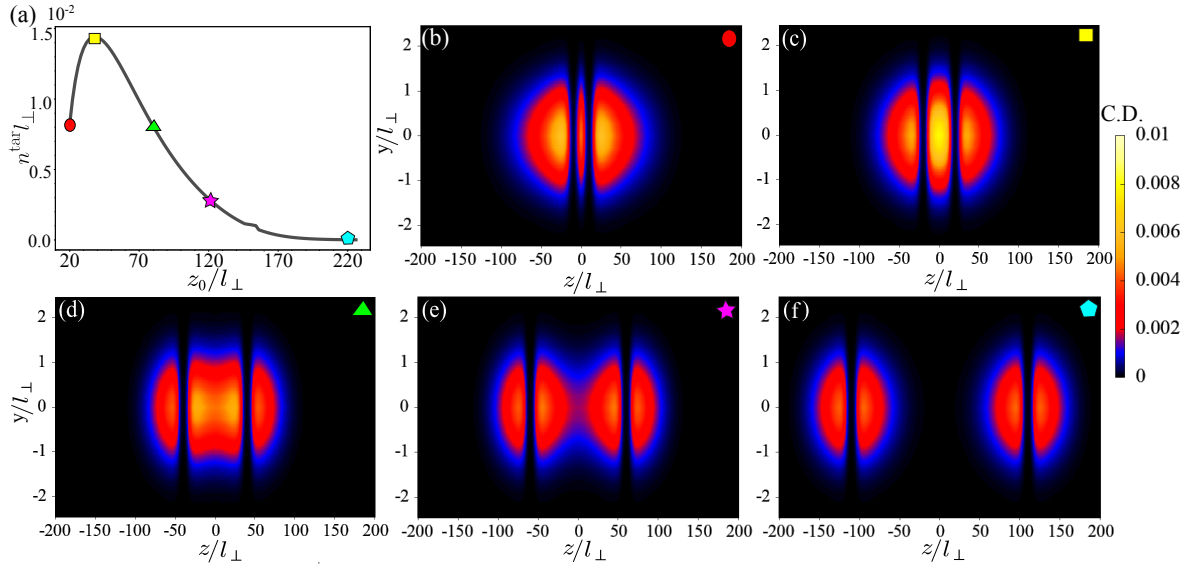


Figure 4. (color online). The density of the target BEC for different separations (z_0) between the two control BECs. (a) The central density of the target BEC as a function of z_0 exhibits a non-monotonous behavior. (b)-(f) shows the ground state density of the target BEC in the yz -plane ($x = 0$) for $z_0 = 20l_\perp$, $z_0 = 40l_\perp$, $z_0 = 80l_\perp$, $z_0 = 120l_\perp$ and $z_0 = 220l_\perp$, respectively. (b)-(d) exhibits three peaks, whereas (e)-(f) possesses four peaks. The other parameters are $\tilde{g}_d = 50$, $\tilde{g} = 210$, $y_0 = 6l_\perp$ and $\lambda = 0.33$. C.D. stands for condensate density.

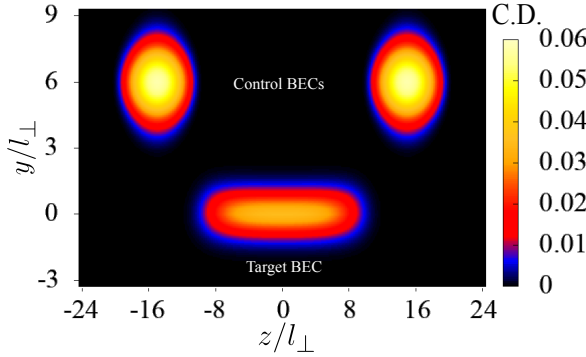


Figure 5. (color online). The condensate density of control and target BECs for $z_0 = 30l_\perp$ and $\lambda = 1$. For control BECs, $\tilde{g}d = 200$ and $\tilde{g} = 840$, and for the target BEC, $\tilde{g}d = 10$ and $\tilde{g} = 42$. C.D. stands for condensate density.

V. SUPERSOLIDS AND INCOHERENT ARRAYS

Finally, we show that having an array of control BECs can imprint a supersolid pattern on the ground state density of the target BEC. In Fig. 6, we show the potential experienced by the target dipole from a periodic array of six control dipoles for different z_0 , where z_0 is now the separation between the adjacent control dipoles. For smaller values of z_0 , the potential has seven local minima [see Fig. 6(a) for $z_0 = 20$]. For significant separation between the control dipoles, as before, each control dipole leads to a pair of local minima and, hence, twelve minima [see Fig. 6(b) for $z_0 = 100$]. The corresponding ground state densities of the target BEC are shown in Fig. 7. For sufficiently small z_0 , we see a seven-peaked structure, with outer density lobes broader than the inner ones

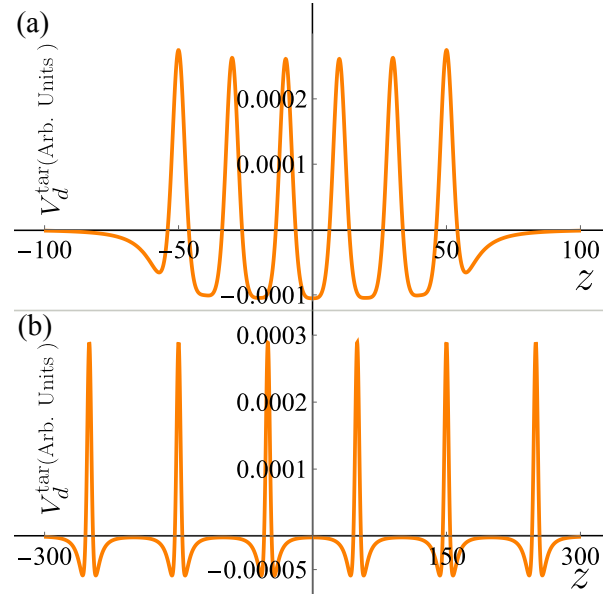


Figure 6. (color online). The dipolar potential $V_d^{\text{tar}}(z)$ (in arbitrary units) acting on the target dipole due to a periodic array of six control dipoles for (a) $z_0 = 20$ and (b) $z_0 = 100$, where z_0 is the separation between adjacent control dipoles. At large z_0 , the total potential can be seen as an array of double-well potentials.

[see Fig. 7(a) for $z_0 = 20l_\perp$]. Increasing z_0 leads to a structural modification in the ground state of target BEC, where the inner lobes become broader than the outer ones [see Fig. 7(b) for $z_0 = 40l_\perp$]. As z_0 increases further, the density lobes develop density modulation, as seen in Figs. 7(c) and 7(d) for $z_0 = 60l_\perp$ and $z_0 = 80l_\perp$. For sufficiently large values of z_0 ,

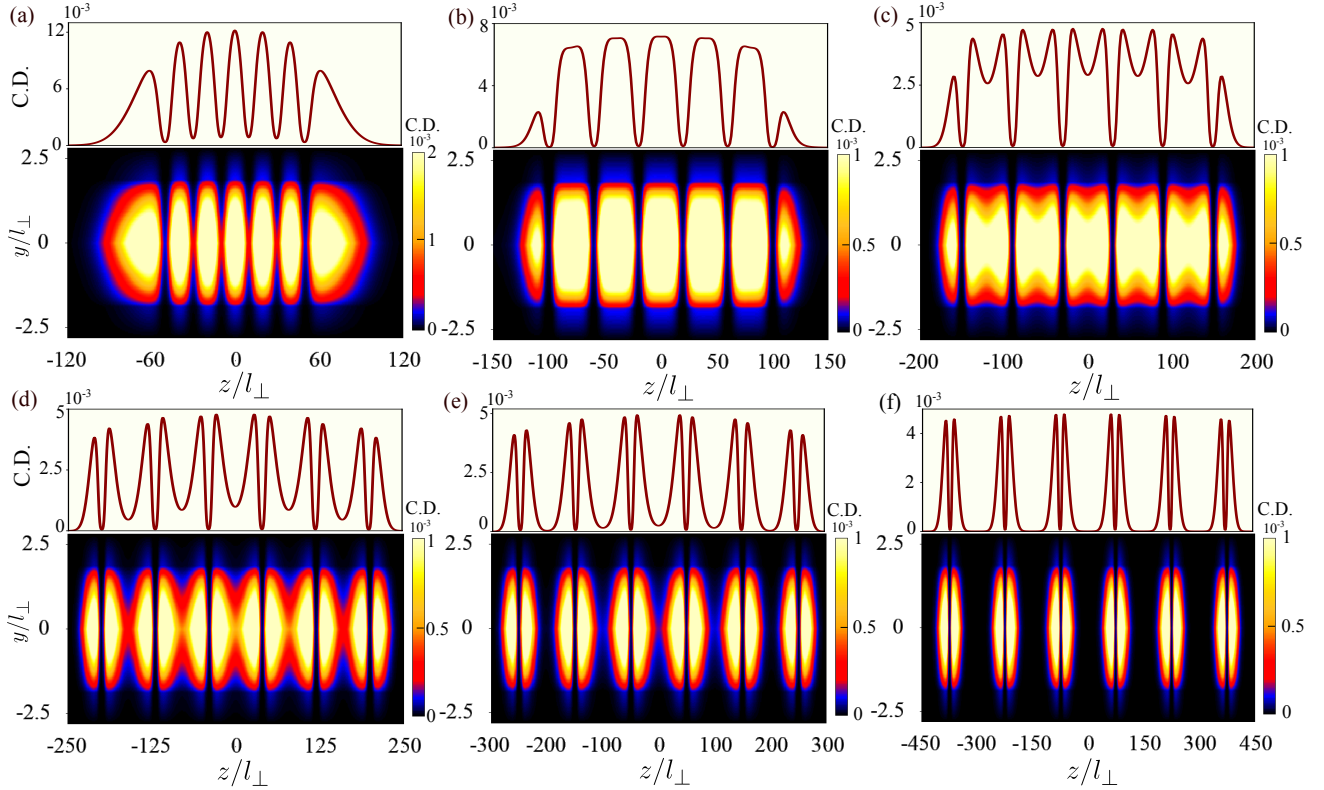


Figure 7. (color online). The density of the target BEC for different values of z_0 in the presence of an periodic array of six control BECs for (a) $z_0 = 20l_\perp$, (b) $z_0 = 40l_\perp$, (c) $z_0 = 60l_\perp$, (d) $z_0 = 80l_\perp$, (e) $z_0 = 100l_\perp$ and (f) $z_0 = 150l_\perp$. The other parameters are $\lambda = 1$, $\tilde{g}d = 50$ and $\tilde{g} = 210$. (a)-(e) are supersolids whereas (f) is an incoherent array of density peaks. C.D. stands for condensate density.

where each of the control dipoles induces a double-well potential on the target dipole along z -axis, we see the formation of an array of double-peak structure [Figs. 7(e) and 7(f) for $z_0 = 100l_\perp$ and $z_0 = 150l_\perp$, respectively].

To quantify the coherence between the density lobes, we calculate Leggett's upper bound of the superfluid fraction [77]:

$$f_s = (2L)^2 \left[\int_{-L}^L dz \tilde{n}(z) \int_{-L}^L \frac{dz}{\tilde{n}(z)} \right]^{-1}, \quad (3)$$

where $\tilde{n}(z)$ is the column density obtained after the radial integration, and the length $2L$ encloses the central region. We see that f_s exhibits a non-trivial dependence on z_0 . For the patterns in Figs. 7(a)-7(e), $f_s > 0.1$, indicating a sufficient superfluid flow between the density lobes to establish the coherence and hence, form a supersolid. For the patterns in Figs. 7(a)-7(c), the distance $2L$ encloses the three density lobes in the center, whereas for the last three patterns, a pair of double-peak structures at the center is taken. The pattern in Fig. 7(a) for $z_0 = 20l_\perp$ has $f_s = 0.448$, and f_s decreases to 0.193 for $z_0 = 40l_\perp$ in Fig. 7(b). Once the density modulation develops in density lobes, f_s increases again. For instance, $f_s = 0.227$ and $f_s = 0.344$ for $z_0 = 60l_\perp$ and $z_0 = 80l_\perp$, respectively for the cases in Figs. 7(c) and 7(d). As the modulation grows into a nodal plane for larger z_0 , f_s starts to decline again, as seen in Fig. 7(e) for which $f_s = 0.272$. For $z_0 = 150l_\perp$, we get $f_s = 0.005$, indicating an incoherent array of density peaks.

VI. EXPERIMENTAL PARAMETERS

Here, we provide the technical details for the state-of-the-art dipolar BECs such as chromium (Cr) [78, 79], erbium (Er) [80–82] and dysprosium (Dy) [83]. We fix the radial trap frequency for all setups to be $\omega_\perp = 2\pi \times 100\text{Hz}$. For Figs. 2, 4 and 7, $\tilde{g} = 210$, and $\tilde{g}_d = 50$, which corresponds to $N = 29000$ (Cr), 3700 (Er) and 1900 (Dy), and $a_s/a_0 = 15.2$ (Cr), 66.5 (Er) and 131.8 (Dy) for both target and control BECs, where a_0 is the Bohr radius. In Fig. 2, we have assumed different numbers of atoms for target and control BECs, which would correspond to ($N_c = 116000, N_t = 5800$) for Cr, ($N_c = 14770, N_t = 740$) for Er and ($N_c = 7500, N_t = 380$) for Dy. The scattering lengths are the same as above.

VII. SUMMARY AND OUTLOOK

To summarize, utilizing the inter-condensate DDIs, we showed that the density of a target BEC can be axially confined and engineered using an array of control BECs. Each control BEC induces a double-well potential on the target BEC. Strikingly, it is possible to realize a supersolid pattern without quantum stabilization. As a function of separation between the adjacent control BECs, we observed a transition between supersolids of different periodicity, one twice the pe-

riodicity of the other. Notably, the supersolid patterns we obtained here differ remarkably from those predicted and observed so far in dipolar condensates, for which quantum stabilization was necessary.

Our studies also open up several perspectives. They can be extended to different spatial arrangements of control BECs, including a two-dimensional (2D) array and exploring its effects on the target BEC. Also, it is interesting to see if a 2D confinement of the target BEC can be attained using control dipolar BECs. Later, one should explore the same on multiple target BECs. The same ideas can also be developed for other dipolar systems; for instance, it may be possible to axially confine or manipulate a Rydberg atom possessing an electric dipole moment using a trapped polar molecule or vice versa. That means utilizing the long-range nature of DDIs to observe

novel phenomena in hybrid systems.

VIII. ACKNOWLEDGEMENTS

We thank C. Mishra for the discussions during the initial stages of the work. We acknowledge National Supercomputing Mission (NSM) for providing computing resources of "PARAM Brahma" at IISER Pune, which is implemented by C-DAC and supported by the Ministry of Electronics and Information Technology (MeitY) and Department of Science and Technology (DST), Government of India. P. N. acknowledges the funding from DST India through an INSPIRE scholarship. R.N. further acknowledges DST-SERB for Swarnajayanti fellowship File No. SB/SJF/2020-21/19, and the MATRICS grant (MTR/2022/000454) from SERB, Government of India.

-
- [1] M. A. Baranov, *Physics Reports* **464**, 71 (2008).
 - [2] T. Lahaye, C. Menotti, L. Santos, M. Lewenstein, and T. Pfau, *Reports on Progress in Physics* **72**, 126401 (2009).
 - [3] M. A. Baranov, M. Dalmonte, G. Pupillo, and P. Zoller, *Chemical Reviews* **112**, 5012 (2012).
 - [4] N. Defenu, T. Donner, T. Macrì, G. Pagano, S. Ruffo, and A. Trombettoni, *Rev. Mod. Phys.* **95**, 035002 (2023).
 - [5] P. Pedri and L. Santos, *Phys. Rev. Lett.* **95**, 200404 (2005).
 - [6] I. Tikhonenkov, B. A. Malomed, and A. Vardi, *Phys. Rev. Lett.* **100**, 090406 (2008).
 - [7] R. Nath, P. Pedri, and L. Santos, *Phys. Rev. Lett.* **102**, 050401 (2009).
 - [8] M. Raghunandan, C. Mishra, K. Łakomy, P. Pedri, L. Santos, and R. Nath, *Phys. Rev. A* **92**, 013637 (2015).
 - [9] C. Mishra and R. Nath, *Phys. Rev. A* **94**, 033633 (2016).
 - [10] L. Chomaz, I. Ferrier-Barbut, F. Ferlaino, B. Laburthe-Tolra, B. L. Lev, and T. Pfau, *Reports on Progress in Physics* **86**, 026401 (2023).
 - [11] H. Kadau, M. Schmitt, M. Wenzel, C. Wink, T. Maier, I. Ferrier-Barbut, and T. Pfau, *Nature* **530**, 194 (2016).
 - [12] I. Ferrier-Barbut, H. Kadau, M. Schmitt, M. Wenzel, and T. Pfau, *Phys. Rev. Lett.* **116**, 215301 (2016).
 - [13] L. Chomaz, S. Baier, D. Petter, M. J. Mark, F. Wächtler, L. Santos, and F. Ferlaino, *Phys. Rev. X* **6**, 041039 (2016).
 - [14] M. Schmitt, M. Wenzel, F. Böttcher, I. Ferrier-Barbut, and T. Pfau, *Nature* **539**, 259 (2016).
 - [15] D. Baillie, R. M. Wilson, R. N. Bisset, and P. B. Blakie, *Phys. Rev. A* **94**, 021602 (2016).
 - [16] M. Schmidt, L. Lassabièvre, G. Quéméner, and T. Langen, *Phys. Rev. Res.* **4**, 013235 (2022).
 - [17] F. Wächtler and L. Santos, *Phys. Rev. A* **93**, 061603 (2016).
 - [18] C. Mishra, L. Santos, and R. Nath, *Phys. Rev. Lett.* **124**, 073402 (2020).
 - [19] M. Sohmen, C. Politi, L. Klaus, L. Chomaz, M. J. Mark, M. A. Norcia, and F. Ferlaino, *Phys. Rev. Lett.* **126**, 233401 (2021).
 - [20] L. Chomaz, D. Petter, P. Ilzhöfer, G. Natale, A. Trautmann, C. Politi, G. Durastante, R. M. W. van Bijnen, A. Patscheider, M. Sohmen, M. J. Mark, and F. Ferlaino, *Phys. Rev. X* **9**, 021012 (2019).
 - [21] L. Tanzi, E. Lucioni, F. Famà, J. Catani, A. Fioretti, C. Gabbanini, R. N. Bisset, L. Santos, and G. Modugno, *Phys. Rev. Lett.* **122**, 130405 (2019).
 - [22] F. Böttcher, J.-N. Schmidt, M. Wenzel, J. Hertkorn, M. Guo, T. Langen, and T. Pfau, *Phys. Rev. X* **9**, 011051 (2019).
 - [23] M. Guo, F. Böttcher, J. Hertkorn, J.-N. Schmidt, M. Wenzel, H. P. Büchler, T. Langen, and T. Pfau, *Nature* **574**, 386 (2019).
 - [24] L. Tanzi, S. M. Rocuzzo, E. Lucioni, F. Famà, A. Fioretti, C. Gabbanini, G. Modugno, A. Recati, and S. Stringari, *Nature* **574**, 382 (2019).
 - [25] P. Ilzhöfer, M. Sohmen, G. Durastante, C. Politi, A. Trautmann, G. Natale, G. Morpurgo, T. Giamarchi, L. Chomaz, M. J. Mark, and F. Ferlaino, *Nature Physics* **17**, 356 (2021).
 - [26] G. Natale, R. M. W. van Bijnen, A. Patscheider, D. Petter, M. J. Mark, L. Chomaz, and F. Ferlaino, *Phys. Rev. Lett.* **123**, 050402 (2019).
 - [27] J. Hertkorn, J.-N. Schmidt, F. Böttcher, M. Guo, M. Schmidt, K. S. H. Ng, S. D. Graham, H. P. Büchler, T. Langen, M. Zwierlein, and T. Pfau, *Phys. Rev. X* **11**, 011037 (2021).
 - [28] L. Tanzi, J. G. Maloberti, G. Biagioni, A. Fioretti, C. Gabbanini, and G. Modugno, *Science* **371**, 1162 (2021).
 - [29] M. A. Norcia, C. Politi, L. Klaus, E. Poli, M. Sohmen, M. J. Mark, R. N. Bisset, L. Santos, and F. Ferlaino, *Nature* **596**, 357 (2021).
 - [30] T. Bland, E. Poli, C. Politi, L. Klaus, M. A. Norcia, F. Ferlaino, L. Santos, and R. N. Bisset, *Phys. Rev. Lett.* **128**, 195302 (2022).
 - [31] K. Mukherjee and S. M. Reimann, *Phys. Rev. A* **107**, 043319 (2023).
 - [32] N. Henkel, R. Nath, and T. Pohl, *Phys. Rev. Lett.* **104**, 195302 (2010).
 - [33] Z.-K. Lu, Y. Li, D. S. Petrov, and G. V. Shlyapnikov, *Phys. Rev. Lett.* **115**, 075303 (2015).
 - [34] D. Baillie and P. B. Blakie, *Phys. Rev. Lett.* **121**, 195301 (2018).
 - [35] J. Hertkorn, J.-N. Schmidt, M. Guo, F. Böttcher, K. S. H. Ng, S. D. Graham, P. Uerlings, T. Langen, M. Zwierlein, and T. Pfau, *Phys. Rev. Res.* **3**, 033125 (2021).
 - [36] E. Poli, T. Bland, C. Politi, L. Klaus, M. A. Norcia, F. Ferlaino, R. N. Bisset, and L. Santos, *Phys. Rev. A* **104**, 063307 (2021).
 - [37] L. E. Young-S. and S. K. Adhikari, *Phys. Rev. A* **105**, 033311 (2022).
 - [38] R. Ghosh, C. Mishra, L. Santos, and R. Nath, *Phys. Rev. A* **106**, 063318 (2022).

- [39] K. Mukherjee, M. N. Tengstrand, T. A. Cardinale, and S. M. Reimann, *Phys. Rev. A* **108**, 023302 (2023).
- [40] C. Mishra, S. Ostermann, F. Mivehvar, and B. P. Venkatesh, *Phys. Rev. A* **107**, 023312 (2023).
- [41] C. Kollath, J. S. Meyer, and T. Giamarchi, *Phys. Rev. Lett.* **100**, 130403 (2008).
- [42] Y.-P. Huang and D.-W. Wang, *Phys. Rev. A* **80**, 053610 (2009).
- [43] R. M. Lutchyn, E. Rossi, and S. Das Sarma, *Phys. Rev. A* **82**, 061604 (2010).
- [44] M. Knap, E. Berg, M. Ganahl, and E. Demler, *Phys. Rev. B* **86**, 064501 (2012).
- [45] N. Matveeva, A. Recati, and S. Stringari, *The European Physical Journal D* **65**, 219 (2011).
- [46] A. Gallemi, M. Guilleumas, R. Mayol, and M. Pi, *Journal of Physics: Conference Series* **497**, 012035 (2014).
- [47] M. Klawunn and L. Santos, *Phys. Rev. A* **80**, 013611 (2009).
- [48] C.-C. Huang and W.-C. Wu, *Phys. Rev. A* **82**, 053612 (2010).
- [49] A. Maluckov, G. Gligorić, L. c. v. Hadžievski, B. A. Malomed, and T. Pfau, *Phys. Rev. A* **87**, 023623 (2013).
- [50] R. Nath, P. Pedri, and L. Santos, *Phys. Rev. A* **76**, 013606 (2007).
- [51] P. Köberle and G. Wunner, *Phys. Rev. A* **80**, 063601 (2009).
- [52] K. Łakomy, R. Nath, and L. Santos, *Phys. Rev. A* **86**, 013610 (2012).
- [53] K. Łakomy, R. Nath, and L. Santos, *Phys. Rev. A* **85**, 033618 (2012).
- [54] K. M. Elhadj, A. Boudjemâa, and U. Al-Khawaja, *Physica Scripta* **94**, 085402 (2019).
- [55] G. Hegde, P. Nayak, R. Ghosh, and R. Nath, *J. Phys. B: At., Mol. Opt. Phys.* **54**, 205301 (2021).
- [56] K. Łakomy, R. Nath, and L. Santos, *Phys. Rev. A* **86**, 023620 (2012).
- [57] S. Müller, J. Billy, E. A. L. Henn, H. Kadau, A. Griesmaier, M. Jona-Lasinio, L. Santos, and T. Pfau, *Phys. Rev. A* **84**, 053601 (2011).
- [58] R. M. Wilson and J. L. Bohn, *Phys. Rev. A* **83**, 023623 (2011).
- [59] L. Du, P. Barral, M. Cantara, J. de Hond, Y.-K. Lu, and W. Ketterle, “Atomic physics on a 50 nm scale: Realization of a bilayer system of dipolar atoms,” (2023), arXiv:2302.07209 [cond-mat.quant-gas].
- [60] D.-W. Wang, M. D. Lukin, and E. Demler, *Phys. Rev. Lett.* **97**, 180413 (2006).
- [61] D.-W. Wang, *Phys. Rev. Lett.* **98**, 060403 (2007).
- [62] C. Trefzger, C. Menotti, and M. Lewenstein, *Phys. Rev. Lett.* **103**, 035304 (2009).
- [63] J. R. Armstrong, N. T. Zinner, D. V. Fedorov, and A. S. Jensen, *Europhysics Letters* **91**, 16001 (2010).
- [64] A. Pikovski, M. Klawunn, G. V. Shlyapnikov, and L. Santos, *Phys. Rev. Lett.* **105**, 215302 (2010).
- [65] D. Hufnagl and R. E. Zilllich, *Phys. Rev. A* **87**, 033624 (2013).
- [66] A. Safavi-Naini, Ş. Söyler, G. Pupillo, H. R. Sadeghpour, and B. Capogrosso-Sansone, *New Journal of Physics* **15**, 013036 (2013).
- [67] M. Rosenkranz, Y. Cai, and W. Bao, *Phys. Rev. A* **88**, 013616 (2013).
- [68] A. Macia, G. E. Astrakharchik, F. Mazzanti, S. Giorgini, and J. Boronat, *Phys. Rev. A* **90**, 043623 (2014).
- [69] F. Cinti, D.-W. Wang, and M. Boninsegni, *Phys. Rev. A* **95**, 023622 (2017).
- [70] A. Boudjemâa and R. Keltoum, *Chaos, Solitons & Fractals* **131**, 109543 (2020).
- [71] S. Bandyopadhyay, H. Sable, D. Gaur, R. Bai, S. Mukerjee, and D. Angom, *Phys. Rev. A* **106**, 043301 (2022).
- [72] D. Edler, C. Mishra, F. Wächtler, R. Nath, S. Sinha, and L. Santos, *Phys. Rev. Lett.* **119**, 050403 (2017).
- [73] A. Pricoupenko and D. S. Petrov, *Phys. Rev. A* **103**, 033326 (2021).
- [74] T. Bland, E. Poli, L. A. P. n. Ardila, L. Santos, F. Ferlaino, and R. N. Bisset, *Phys. Rev. A* **106**, 053322 (2022).
- [75] S. Li, U. N. Le, and H. Saito, *Phys. Rev. A* **105**, L061302 (2022).
- [76] A. Guttridge, D. K. Ruttle, A. C. Baldoock, R. González-Férez, H. R. Sadeghpour, C. S. Adams, and S. L. Cornish, *Phys. Rev. Lett.* **131**, 013401 (2023).
- [77] A. J. Leggett, *Phys. Rev. Lett.* **25**, 1543 (1970).
- [78] A. Griesmaier, J. Werner, S. Hensler, J. Stuhler, and T. Pfau, *Phys. Rev. Lett.* **94**, 160401 (2005).
- [79] Q. Beaufils, R. Chicireanu, T. Zanon, B. Laburthe-Tolra, E. Maréchal, L. Vernac, J.-C. Keller, and O. Gorceix, *Phys. Rev. A* **77**, 061601 (2008).
- [80] K. Aikawa, A. Frisch, M. Mark, S. Baier, A. Rietzler, R. Grimm, and F. Ferlaino, *Phys. Rev. Lett.* **108**, 210401 (2012).
- [81] R. Song, S.-H. Zhang, W.-M. Liao, J. Wang, S.-J. Deng, and H.-B. Wu, *Results in Physics* **52**, 106795 (2023).
- [82] B. Seo, Z. Chen, M. Huang, M. K. Parit, Y. He, P. Chen, and G.-B. Jo, *Journal of the Korean Physical Society* **82**, 901 (2023).
- [83] M. Lu, N. Q. Burdick, S. H. Youn, and B. L. Lev, *Phys. Rev. Lett.* **107**, 190401 (2011).